Communications in Computational Chemistry
Commun. Comput. Chem. Vol. 8, No. 1, 37–43
doi: 10.4208/cicc.2025.358.01
Regular Article

VBData: A Valence Bond Property Dataset of Single Bonds for Organic Compounds

Mingwei Yang[1], Yameng Zheng[1], Muhammad Shoaib[1], Wei Wu[2,*] and Jinshuai Song[1,*]

[1] *College of Chemistry, Pingyuan Laboratory, and State Key Laboratory of Cotton Bio-breeding and Integrated Utilization, Zhengzhou University, Zhengzhou, Henan 450001, China;*
[2] *State Key Laboratory of Physical Chemistry of Solid Surfaces, Fujian Provincial Key Laboratory of Theoretical and Computational Chemistry, and College of Chemistry and Chemical Engineering, Xiamen University, Xiamen, Fujian 361005, China.*

[*] Corresponding authors: weiwu@xmu.edu.cn; jssong@zzu.edu.cn.

Received 24 Dec. 2025; Accepted (in revised version) 17 Feb. 2026

Abstract: The properties of valence bonds are fundamental to understand and predict the reactivity of chemical reactions. This article presents a comprehensive dataset derived from quantum chemical calculations performed at a consistent computational level for more than 40,000 organic compounds (containing only C, H, N, and O atoms) and over 400,000 non-cyclic single bonds within them. Key bond properties include resonance energies and structural weights. The valence bond computation was performed using XMVB program at the VBSCF level, based on the equilibrium geometries optimized at the B3LYP/def2-SVP level. This dataset is anticipated to serve as a new standard benchmark for bond properties in organic chemistry and to provide a foundation for developing machine learning models.

Key words: bond dataset, valence bond theory, resonance energy, VBData, structural weights.

1. Introduction

Chemical bond properties are significant in predicting the chemical reactivity and selectivity of chemical reactions [1-4]. Key descriptors such as bond length, bond order, bond dissociation energy (BDE), and acid dissociation constant (pKa) could be obtained from thermodynamic experiments or quantum chemical calculations. Among these, valence bond (VB) properties serve as crucial indicators of molecular kinetic stability [5-7], aromaticity [8-10], magnetic behavior [11], and chemical reactivity [12,13]. Compared to thermochemical experiments and quantum chemistry based on molecular orbital based quantum chemistry, valence bond (VB) theory offers superior intuitive insights into chemical bonding. It provides a clear physical explanation for bond strength and directionality, which facilitates the understanding of molecular stability and chemical reactions. Traditional quantum chemical methods based on valence bond theory can accurately predict diverse molecular properties but require high computational cost. These limitations consequently restrict the application of VB methods to rapid screening of functional molecules in realistic chemical systems.

The prediction of bond properties could be achieved by machine learning models, driven by the continuous advancement of artificial intelligence [14-17]. Machine learning can uncover latent relationships between feature descriptors and properties, overcoming the limitations of conventional methods. Machine learning is extensively applied across domains, benefiting from its rapid processing and user-friendly nature. These machine learning models rely on corresponding chemical property databases. However, existing datasets still exhibit critical gap in coverage and applicability. To date, several high-quality chemical datasets (e.g., ioChem-BD [18], BDE-db [19,20], iBOND, BDNCM [1], and the QM series [21,22]) have been developed and made publicly available to support machine learning models and research in chemical property prediction. Nevertheless, most datasets are highly specialized and thus unsuitable for general use. Additionally, the lack of high-quality datasets to support model training has left the domain of valence bond property largely unexplored.

In modern valence bond theory, the description of a single bond between atoms A and B requires a superposition of multiple resonance structures, as shown in **Figure 1**.

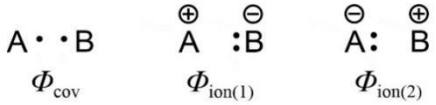

Figure 1. Three resonance structures of a single bond.

As shown in Eq. (1), the VB wavefunction Ψ is expressed as a combination of the covalent form $\Phi_{cov}(A\cdot\text{-}\cdot B)$ and two ionic forms, $\Phi_{ion}(A^+B^-)$ and Φ'_{ion} (A^-B^+) [23,24]:

$$\Psi=C_1\Phi_{cov}+C_2\Phi_{ion}+C_3\Phi'_{ion} \quad (1)$$

The resonance energy (RE) [25,26] can be determined via thermochemical methods [27], hydrogenation heat experiments, or quantum chemical calculations [28]. However, experimental determination of resonance energy for polyatomic molecules remains technically challenging and cost-prohibitive. The resonance energy [29] is defined as the energy difference between the lowest-energy structure and the full wavefunction described by Eq. (1). For the small organic molecules studied in this work, the covalent structure exhibits a relatively low energy. Thus, the single-bond RE is calculated as Eq. (2) [30]:

$$RE = E(\Phi_{cov}) - E_\Psi \quad (2)$$

where E_Ψ is the energy of the total wavefunction (Ψ) and $E(\Phi_{cov})$ is the energy of the most stable structure, which represents the energy of the covalent structure in this study.

The overall stability arises from a superposition of resonance structures, each assigned a specific weight that quantifies its contribution (**Figure 1**). The normalized structural weight in Valence Bond Self-Consistent Field (VBSCF) [31] method is defined as [32]:

$$W_K = C_K\langle\Phi_K|\Psi\rangle=\sum_L C_K M_{KL} C_L \quad (3)$$

where W_K denotes the structural weight, C_K and C_L are the structural coefficients in the wavefunction, and M_{KL} represents overlap matrices between K and L structures. This study focuses on nine key chemical bond types (C-H, C-C, H-N, C-N, C-O, H-O, N-O, N-N and O-O), all of which are suitable for computational simulation with the present VB model [30].

In this article, we report a dataset called VBData including the valence bond properties of single bonds for organic compounds. The dataset has 40,837 organic compounds and 400,972 chemical bonds, with systematic documentation of their valence bond properties. All molecular geometries were optimized at the B3LYP/def2-SVP theoretical level [33,34], following bond property calculations by using the VBSCF [31] method. This computational protocol was carefully selected to achieve an optimal balance between accuracy and computational efficiency. The multidimensional information effectively captures both the bond strength characteristics and chemical reactivity profiles of the investigated bonds. We expect graph neural network (GNN) [35] models to be applied for valence bond property prediction based on this dataset.

2. Theoretical method

2.1 Molecular and chemical bond selection criteria.

The molecular structures were sourced from the same PubChem Compound database [36] utilized by BDE-db. Selection criteria included neutral organic molecules containing fewer than 10 heavy atoms (excluding hydrogen) and composed exclusively of C, H, O, N. All SMILES strings were standardized and deduplicated using RDKit [37].

2.2 Conformational optimization.

Initial molecular geometries were generated from SMILES strings using RDKit. Notably, while the default 3D conformation generation excludes hydrogen atoms, we explicitly added hydrogen atoms prior to optimization due to their critical influence on molecular conformation. To enhance the quality of 3D conformers, we adopted a hierarchical workflow as shown in **Figure 2**. Firstly, 500 conformers for every molecule were generated using the ETKDG method [38]. Next, these conformers were optimized by the MMFF94 force field [39]. Subsequently, the lowest-energy conformation was selected as the initial geometry for subsequent high-level optimizations. The obtained geometry was exported to an XYZ file and further optimized by using the semi-empirical ODM3 [40] method within the MNDO [41] quantum chemical program to improve structural accuracy and reduce computational overhead in later stages. Final geometry was optimized at the B3LYP/def2-SVP level in Gaussian 16 [42] (computational details of structure optimization are provided in the Supporting Information S1-S2). All Gaussian optimized structures were rigorously verified for energy convergence.

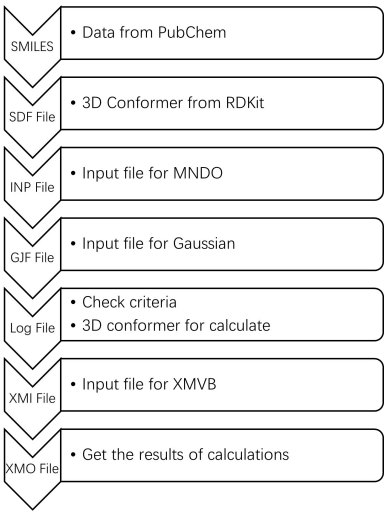

Figure 2. Overview of the workflow for this work, including the software and files utilized.

2.3 Valence bond calculations.

To maximize the diversity of bond types per unit of computational effort and avoid complex intramolecular interactions in strained rings, such as ring strain, non-cyclic single bonds that are not in rings were selected from the optimized molecular structures for data collection, to enable the systematic construction of a comprehensive dataset. The valence-bond properties of bonds in rings are strongly influenced by the ring structure and the local chemical environment, resulting in a broad distribution that poses significant challenges for effective sampling. These bonds were calculated by using the XMVB program [43,44], to collect structural weights and resonance energy. The computational procedures are depicted in **Figure 2**. For each targeted bond, two separate XMVB calculations were performed to compute E_Ψ by 3 structures and $E(\Phi_{cov})$ by the covalent structure. The active space was defined with 2 active orbitals in 2 active

electrons for the non-cyclic single bond. Inactive orbitals are orbitals that remain doubly occupied by the remaining electrons in all structures. The inactive orbitals are also optimized in VBSCF to provide the environmental contribution to the target single bond. Fragment orbitals constructed from hybrid atomic orbitals (HAOs) were employed. The initial guess was used as the program default, which automatically provides a starting wave function by diagonalizing the fragment-localized Fock matrix of molecular orbitals. VB structures (including the covalent-only structure) were generated automatically by XMVB based on the specified keywords. The energy convergence threshold was set to 10^{-7}. Details and representative examples of the XMVB calculations are provided in the Supporting Information (S3). The total energies were read from two output files to calculate the RE by Eq. (2).

Table 1. The items and descriptions in the dataset.

Item	Description
rid	Index of data entry
SMILES	Simplified Molecular Input Line Entry System, Molecular 2D representation.
Fragment1	Canonical SMILES of the first fragments generated by the breaking of chemical bonds.
Fragment2	Canonical SMILES of the second fragments generated by the breaking of chemical bonds.
Bond_index	Index of chemical bond in the molecule.
Begin_idx	Index of the first bonded atom in the whole molecule.
Begin_atom	Element symbol of the first bonded atom (e.g., C, N, O, H).
End_idx	Index of the second bonded atom in the whole molecule.
End_atom	Element symbol of the second bonded atom (e.g., C, N, O, H).
Bond type	Type of chemical bond, such as C-C, C-H, C-N, N-H.
RE	Resonance energy of the chemical bond, specified to 2 decimal places in kcal mol^{-1}.
Weight_1	Weight of covalent structure in resonance structures, specified to 2 decimal places.
Weight_2	Weight of ionic structure in resonance structures, specified to 2 decimal places.
Weight_3	Weight of another ionic structure in resonance structures, specified to 2 decimal places.

2.4 Technical validation.

To ensure the physical reliability of our computational results, a systematic validation protocol was implemented across all stages. This included error analysis, convergence verification, and examination of vibrational frequencies. Starting from an initial set of 45,051 molecules for geometry optimization, convergence failure was examined. Specifically, 400 molecules were discarded due to failed optimizations, and 420 were excluded with imaginary frequencies. Furthermore, all instances where XMVB bond-property calculations failed to complete normally were also filtered out, including the removal of 3,394 molecules. Overall, the final dataset was rigorously screened to comprise only entries fulfilling all convergence and stability requirements, to ensure a high standard of reliability for downstream investigations. The compiled dataset is composed of valence bond properties for 400,972 non-cyclic single bonds derived from 40,837 organic compounds.

3. Results and discussion

3.1 Data records

The dataset is stored in CSV (Comma-Separated Values) format and contains the following fields: SMILES strings, molecular fragments, bond indices, bond types, bond resonance energies, and weights of resonance structures. For each bond, the valence bond properties include its resonance energy and the respective weights of the three resonance structures. These items were collected from geometry optimization and XMVB computations. The definitions of all column headers are explicitly detailed in **Table 1**. Atom and bond indices are defined as the default zero-based order generated by RDKit when processing the molecular SMILES. RDKit canonicalization was applied to the SMILES representations of all molecules and fragments.

Table 2. Distribution of molecules and chemical bonds by number of heavy atoms.

#Heavy Atoms	Molecules	Chemical bonds
1	1	4
2	6	26
3	33	153
4	131	714
5	444	2,838
6	1,254	9,509
7	3,327	29,355
8	7,323	70,471
9	13,165	131,307
10	15,153	156,595

3.2 Data distribution

The molecular structures in VBData comprise various numbers of heavy atoms (non-hydrogen atoms). **Table 2** provides a

statistical summary of the distribution of molecules across different heavy-atom counts.

As expected, both the number of molecules and the total number of chemical bonds increase with the number of heavy atoms. Correspondingly, molecules and bonds associated with higher heavy-atom counts constitute a progressively larger proportion of the dataset. This trend reflects the greater structural complexity and increased bonding possibilities inherent to larger molecules. Additionally, the composition of the dataset is further analyzed with respect to different bond types.

Table 3. Number of samples categorized by chemical bond type.

Bond type	Count	Percentage
C-H	288,800	72.03%
C-C	43,964	10.96%
H-N	24,451	6.10%
C-N	16,291	4.06%
C-O	14,939	3.73%
H-O	9,989	2.49%
N-O	1,229	0.31%
N-N	1,068	0.27%
O-O	241	0.06%

The distribution of chemical bond types is summarized in **Table 3**. C–H bonds constitute the dominant category, accounting for over 72% of the total. Collectively, C–C, C–O, and C–N bonds represent more than 18%. In contrast, bonds not involving carbon are far less frequent, comprising less than 10% and thus forming only a minor fraction of the dataset. This distribution is a direct reflection of the characteristic composition and bonding patterns found in organic molecules. For optimal utilization of this dataset, we suggest employing a stratified approach based on chemical bond type.

Table 4. Statistical summary of the VBData.

	RE (kcal mol^{-1})	Weight1	Weight2	Weight3
Mean	13.07	0.72	0.16	0.11
Std	10.25	0.03	0.04	0.04
Min	1.07	0.57	0.01	0.01
25%	7.97	0.71	0.15	0.10
50%	8.35	0.74	0.15	0.10
75%	16.69	0.74	0.16	0.11
Max	84.77	0.89	0.40	0.41

The key statistical characteristics of the dataset are summarized in **Table 4**, which reports the mean, standard deviation (std), minimum (min), maximum (max), and the 25th, 50th (median), and 75th percentiles for each of the primary valence bond properties investigated. The Resonance Energy (RE) shows a broad distribution with a mean of 13.07 kcal mol^{-1} and a substantial standard deviation of 10.25 kcal mol^{-1}. The values range widely from a minimum of 1.07 kcal mol^{-1} to a maximum of 84.77 kcal mol^{-1}. The median RE (8.35 kcal mol^{-1}) is lower than the mean, indicating a right-skewed distribution where a smaller number of structures possess significantly higher RE values.

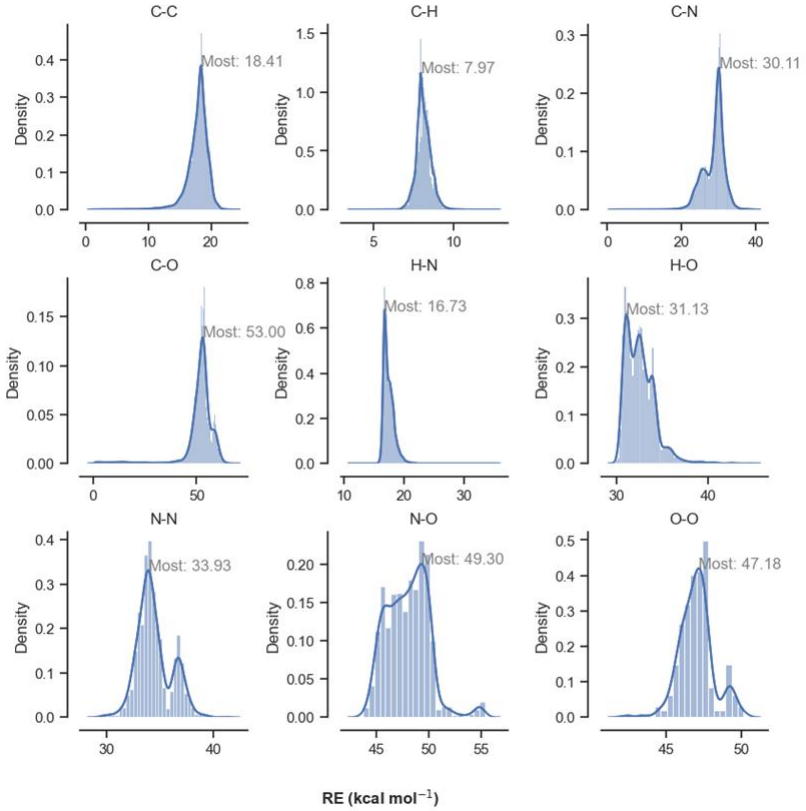

Figure 3. Distribution of resonance energies categorized by chemical bond type, and modal RE values are labeled in grey.

Weights of covalent structure (Weight1) have a high mean contribution of 0.72, with very low variability (Std = 0.03). Its median (0.74) is close to the mean value. In contrast, weights of ionic structures (Weight2 and Weight3) have much smaller mean values (0.16 and 0.11, respectively). For the weight of three structures, the values of 25th, 50th (median), and 75th percentiles are closely clustered, due to the contribution of a huge number of C-H bonds as shown in **Table 3**.

Figure 3 displays the bond resonance energy (RE) distributions for various bond types, with modal values indicated. The highest RE values are observed for bonds containing oxygen and nitrogen. For example, the C–O bond has the highest modal RE at 53.0 kcal mol^{-1}, followed by N–O at 49.3 kcal mol^{-1}, and O–O at 47.2 kcal mol^{-1} bonds. This trend suggests significant ionic characters and strong electrostatic interactions involving the heavy atoms. In contrast, C–C bonds display moderate resonance stabilization (18.41 kcal mol^{-1}), consistent with the low electronegativity difference and polarization between equivalent carbon atoms. Furthermore, C–H bonds have the lowest RE (8.0 kcal mol^{-1}), while H–N and H–O bonds display intermediate REs with 16.7 and 31.1 kcal mol^{-1}. This trend indicates that RE generally increases with the electronegativity difference between the bonded atoms.

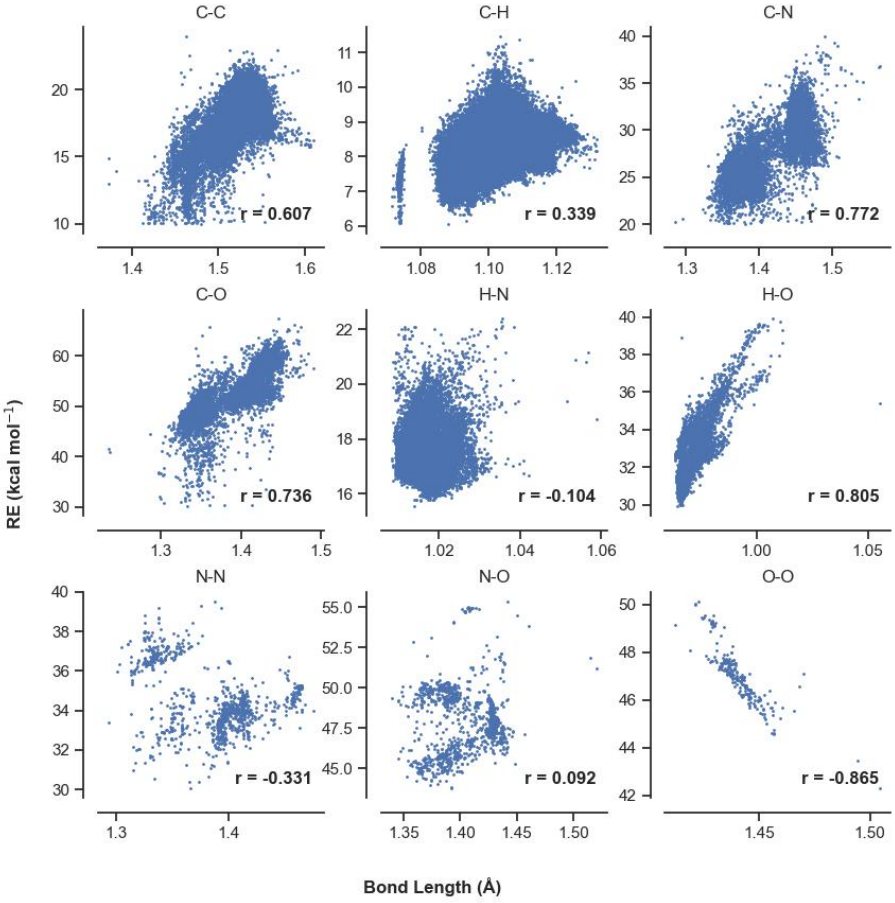

Figure 4. Relationship between resonance energy and bond length categorized by chemical bond type.

A notable feature is the multi-modal distribution for H-O, N–N, N–O and O-O bonds, which suggests the presence of two distinct chemical environments, such as different hybridization states or functional group contexts. For H-O bonds, the bimodal distribution at 31.1 kcal mol^{-1} and 34.1 kcal mol^{-1} likely corresponds to O-H bonds in alcohols (R-OH) and carboxylic acids (RCOOH), respectively. Alcohols exhibit a broader distribution of the values, while the larger RE value (34.1 kcal mol^{-1}) is more frequently observed in carboxylic acids. For N-N bonds, the observed peak at 36.6 kcal mol^{-1} is characteristic of nitrosamines, such as R_2N-N=O. In contrast, other types of N-N bonds, such as those in hydrazine derivatives, primarily exhibit RE values around 33.9 kcal mol^{-1}. The O-O bond distribution shows a small peak at 49.4 kcal mol^{-1} for peroxycarboxylic acids (R-COO-OH). For N-O bonds, peaks are located at 55.2 kcal mol^{-1}, 45.9 kcal mol^{-1}, and 49.3 kcal mol^{-1}, corresponding to alkyl nitrites (RO-N=O), amides (R-$CONH_2$), and oximes (R-C=NOH). Collectively, these results quantify how heteroatom identity and bond polarity govern resonance effects, providing a basis for predicting electronic structure and reactivity.

Figure 4 depicts the correlation between RE and optimized bond length (BL) across nine bond types, along with their respective Pearson correlation coefficient (r). A strong positive correlation is observed for C–C (r = 0.640), C–N (r = 0.739), and H–O (r = 0.831) bonds, indicating that longer BL is associated with resonance stabilization. In contrast, O–O bonds exhibit a strong negative correlation (r = −0.865), where longer bonds correspond to lower RE values. Moderately positive correlations are noted for C–O (r = 0.501) and C–H (r = 0.341) bonds. Notably, H–N (r = −0.099), N–N (r = −0.326), and N–O (r = 0.092) bonds display negligible correlations. It should be noted that these correlations are based on aggregated data

encompassing multiple functional groups and chemical environments. RE in these bonds would be influenced by various factors beyond bond length, such as hybridization, adjacent substituents, or specific electronic environments.

3.3 Data availability

VBData is available at https://github.com/mwyang25/VBData_Gen/tree/main/data. Code is available at https://github.com/mwyang25/VBData_Gen/ used to perform the high-throughput calculations. The code relies on RDKit to process molecular information in Python, Gaussian 16 to perform the DFT calculation, XMVB to perform the valence bond calculation, and Pandas for data processing.

4. Conclusion

This work establishes a systematic dataset of valence bond properties, VBData, which addresses a critical gap in current chemical bond data resources and provides a benchmark for valence bond theory. Generated through a unified computational protocol, the dataset collects key valence bond descriptors, including resonance energies and structural weights and over 400,000 non-cyclic single bonds across more than 40,000 organic compounds. The selected methodology balances between computational accuracy and efficiency, enabling the dataset to reliably capture both bond-strength characteristics and chemical reactivity profiles. VBData is a new standard reference for research on bond properties in organic chemistry. It's a foundational resource for training machine learning models, such as graph neural networks, to train predictive modeling in chemical science.

The current dataset focuses primarily on the valence bond properties of non-cyclic single bonds. In systems with double and triple bonds, molecules have more active electrons and a larger active space, leading to more complex and numerous resonance structures. For instance, a double bond has 20 structures, while a triple bond has 175 structures. As for conjugated systems, Zhou et al. have already constructed a dataset comprising 89 conjugated species, totaling 40,649 structures [45]. Consequently, the increasing complexity of these systems requires more entries to build a dataset. In the future, we plan to extend the dataset to more bond types, including double bonds, triple bonds, and conjugated π-systems, to enhance its scope and practical utility.

Supporting Information

Supporting information can be downloaded here.

Acknowledgments

We acknowledge financial support from the National Natural Science Foundation of China (No. 22173083) and the Fundamental Research Funds of State Key Laboratory of Cotton Bio-breeding and Integrated Utilization (No. CBIU2023ZZ14).

References

[1] Wen M., Blau S.M., Spotte-Smith E.W.C., Dwaraknath S. and Persson K.A., BonDNet: a graph neural network for the prediction of bond dissociation energies for charged molecules. *Chem. Sci.,* **12** (2021), 1858–1868.

[2] Schmidt-Rohr K., Why combustions are always exothermic, yielding about 418 kJ per mole of O2. *J. Chem. Educ.,* **92** (2015), 2094–2099.

[3] Qu X., Latino D.A. and Aires-de-Sousa J., A big data approach to the ultra-fast prediction of DFT-calculated bond energies. *J. Cheminform.,* **5** (2013), 34.

[4] St. John P.C., Guan Y., Kim Y., Kim S. and Paton R.S., Prediction of organic homolytic bond dissociation enthalpies at near chemical accuracy with sub-second computational cost. *Nat. Commun.,* **11** (2020), 2328.

[5] Corderman R.R. and Beauchamp J.L., Quantitative metal-ligand bond dissociation energies in the gas phase by ion cyclotron resonance spectroscopy. *J. Am. Chem. Soc.,* **98** (1976), 3998–4000.

[6] Laconsay C.J., James A.M. and Galbraith J.M., Effect of lone pairs on molecular resonance energy. *J. Phys. Chem. A,* **120** (2016), 8430–8434.

[7] Aihara J., Kinetic stability of metallofullerenes as predicted by the bond resonance energy model. *Phys. Chem. Chem. Phys.,* **3** (2001), 1427–1431.

[8] Aihara J., Topological resonance energy, bond resonance energy, and circuit resonance energy. *J. Phys. Org. Chem.,* **21** (2008), 79–85.

[9] Makino M., Dias J.R. and Aihara J., Bond resonance energy verification of σ-aromaticity in cycloalkanes. *J. Phys. Chem. A,* **124** (2020), 4549–4555.

[10] Dias J.R., Assessment of the performance of the bond resonance energy, circuit resonance energy, magnetic resonance energy, ring currents, and aromaticity of anthracene, biphenylene, phenalenyl, and p-terphenyl. *J. Phys. Chem. A,* **125** (2021), 8482–8497.

[11] James A.M., Laconsay C.J. and Galbraith J.M., Charge-shift corrected electronegativities and the effect of bond polarity and substituents on covalent–ionic resonance energy. *J. Phys. Chem. A,* **121** (2017), 5190–5195.

[12] Aihara J., Bond resonance energy and verification of the isolated pentagon rule. *J. Am. Chem. Soc.,* **117** (1995), 4130–4136.

[13] Jones G.A. and Bradshaw D.S., Resonance energy transfer: from fundamental theory to recent applications. *Front. Phys.,* **7** (2019), 100–119.

[14] Liu Y., Li Y., Yang Q., Yang J., Zhang L. and Luo S., Prediction of bond dissociation energy for organic molecules based on a machine-learning approach. *Chin. J. Chem.,* **42** (2024), 1967–1974.

[15] Mansouri K., Cariello N.F., Korotcov A., Tkachenko V., Grulke C.M., Sprankle C.S., Allen D., Casey W.M., Kleinstreuer N.C. and Williams A.J., Open-source QSAR models for pKa prediction using multiple machine learning approaches. *J. Cheminform.,* **11** (2019), 60.

[16] Johnston R.C., Yao K., Kaplan Z., Chelliah M., Leswing K., Seekins S., Watts S., Calkins D., Chief Elk J., Jerome S.V., Repasky M.P. and Shelley J.C., Epik: pKa and protonation state prediction through machine learning. *J. Chem. Theory Comput.,* **19** (2023), 2380–2388.

[17] Yang Q., Li Y., Yang J., Liu Y., Zhang L., Luo S. and Cheng J., Holistic prediction of the pKa in diverse solvents based on

a machine-learning approach. *Angew. Chem. Int. Ed.,* **59** (2020), 19282–19291.

[18] Álvarez-Moreno M., De Graaf C., López N., Maseras F., Poblet J.M. and Bo C., Managing the computational chemistry big data problem: the ioChem-BD platform. *J. Chem. Inf. Model.,* **55** (2015), 95–103.

[19] [dataset] John P.S., Guan Y., Kim Y. and Kim S., BDE-db: a collection of 290,664 homolytic bond dissociation enthalpies for small organic molecules. *figshare,* (2019), v1.

[20] St. John P.C., Guan Y., Kim Y. and Kim S., Quantum chemical calculations for over 200,000 organic radical species and 40,000 associated closed-shell molecules. *Sci. Data.,* **7** (2020), 244.

[21] Ramakrishnan R., Dral P.O., Rupp M. and von Lilienfeld O.A., Quantum chemistry structures and properties of 134 kilo molecules. *Sci. Data.,* **1** (2014), 140022.

[22] Rupp M., Tkatchenko A., Müller K.R. and von Lilienfeld O.A., Modeling of molecular atomization energies using machine learning. *J. Cheminform.,* **4** (2012), 33.

[23] Shaik S., Danovich D., Wu W. and Hiberty P.C., Charge-shift bonding and its manifestations in chemistry. *Nat. Chem.,* **1** (2009), 443–449.

[24] Song J., Chen Z., Shaik S. and Wu W., An efficient algorithm for complete active space valence bond self-consistent field calculation. *J. Comput. Chem.,* **34** (2013), 38–48.

[25] Liebman J.F. and Greenberg A., The resonance energy of amides and their radical cations. *Struct. Chem.,* **30** (2019), 1631–1634.

[26] Mo Y., The resonance energy of benzene: a revisit. *J. Phys. Chem. A,* **113** (2009), 5163–5169.

[27] Kolesnichenko V.L., Resonance energy of an arene hydrocarbon from heat of combustion measurements. *J. Chem. Educ.,* **92** (2015), 2170–2172.

[28] Parmar K. and Gravel M., Quantifying vertical resonance energy in aromatic systems with natural bond orbitals. *Eur. J. Org. Chem.,* **26** (2023), e202201008.

[29] Shaik S., Maitre P., Sini G. and Hiberty P.C., The charge-shift bonding concept: electron-pair bonds with very large ionic–covalent resonance energies. *J. Am. Chem. Soc.,* **114** (1992), 7861–7866.

[30] Shaik S., Danovich D., Galbraith J.M., Braïda B., Wu W. and Hiberty P.C., Charge-shift bonding: a new and unique form of bonding. *Angew. Chem. Int. Ed.,* **59** (2020), 984–1001.

[31] Van Lenthe J.H. and Balint-Kurti G.G., The valence-bond SCF method: synopsis of theory and test calculation of OH potential energy curve. *Chem. Phys. Lett.,* **76** (1980), 138–142.

[32] Su P., Song L., Wu W., Hiberty P.C. and Shaik S., A valence bond study of the dioxygen molecule. *J. Comput. Chem.,* **28** (2007), 185–197.

[33] Becke A.D., Density-functional thermochemistry. III. The role of exact exchange. *J. Chem. Phys.,* **98** (1993), 5648–5652.

[34] Weigend F. and Ahlrichs R., Balanced basis sets of split valence, triple zeta valence and quadruple zeta valence quality for H to Rn: design and assessment of accuracy. *Phys. Chem. Chem. Phys.,* **7** (2005), 3297–3305.

[35] Battaglia P.W., Hamrick J.B., Bapst V., Sanchez-Gonzalez A., Zambaldi V., Malinowski M., Tacchetti A., Raposo D., Santoro A., Faulkner R., Gulcehre C., Song F., Ballard A., Gilmer J., Dahl G., Vaswani A., Allen K., Nash C., Langston V., Dyer C., Heess N., Wierstra D., Kohli P., Botvinick M., Vinyals O., Li Y. and Pascanu R., Relational inductive biases, deep learning, and graph networks. *arXiv preprint,* **2018**, 1806.01261.

[36] Kim S., Chen J., Cheng T., Gindulyte A., He J., He S., Li Q., Shoemaker B.A., Thiessen P.A., Yu B., Zaslavsky L., Zhang J. and Bolton E.E., PubChem 2019 update: improved access to chemical data. *Nucleic Acids Res.,* **47** (2019), D1102–D1109.

[37] Coley C.W., Green W.H. and Jensen K.F., RDChiral: an RDKit wrapper for handling stereochemistry in retrosynthetic template extraction and application. *J. Chem. Inf. Model.,* **59** (2019), 2529–2537.

[38] Riniker S. and Landrum G.A., Better informed distance geometry: using what we know to improve conformation generation. *J. Chem. Inf. Model.,* **55** (2015), 2562–2574.

[39] Halgren T.A., Merck molecular force field. I. Basis, form, scope, parameterization, and performance of MMFF94. *J. Comput. Chem.,* **17** (1996), 490–519.

[40] Dral P.O., Wu X. and Thiel W., Semiempirical quantum-chemical methods with orthogonalization and dispersion corrections. *J. Chem. Theory Comput.,* **15** (2019), 1743–1760.

[41] Dewar M., Development and status of MNDO/3 and MNDO. *J. Mol. Struct.,* **100** (1983), 41–50.

[42] Frisch M.J., Trucks G.W., Schlegel H.B., Scuseria G.E., Robb M.A., Cheeseman J.R., Scalmani G., Barone V., Petersson G.A., Nakatsuji H., Li X., Caricato M., Marenich A.V., Bloino J., Janesko B.G., Gomperts R., Mennucci B., Hratchian H.P., Ortiz J.V., Izmaylov A.F., Sonnenberg J.L., Williams-Young D., Ding F., Lipparini F., Egidi F., Goings J., Peng B., Petrone A., Henderson T., Ranasinghe D., Zakrzewski V.G., Gao J., Rega N., Zheng G., Liang W., Hada M., Ehara M., Toyota K., Fukuda R., Hasegawa J., Ishida M., Nakajima T., Honda Y., Kitao O., Nakai H., Vreven T., Throssell K., Montgomery J.A. Jr., Peralta J.E., Ogliaro F., Bearpark M.J., Heyd J.J., Brothers E.N., Kudin K.N., Staroverov V.N., Keith T.A., Kobayashi R., Normand J., Raghavachari K., Rendell A.P., Burant J.C., Iyengar S.S., Tomasi J., Cossi M., Millam J.M., Klene M., Adamo C., Cammi R., Ochterski J.W., Martin R.L., Morokuma K., Farkas O., Foresman J.B. and Fox D.J., Gaussian 16 revision B.01. Gaussian, Inc., Wallingford, 2016.

[43] Song L., Mo Y., Zhang Q. and Wu W., XMVB: a program for ab initio nonorthogonal valence bond computations. *J. Comput. Chem.,* **26** (2005), 514–521.

[44] Chen Z., Ying F., Chen X., Song J., Su P., Song L., Mo Y., Zhang Q. and Wu W., XMVB 2.0: a new version of Xiamen valence bond program. *Int. J. Quantum Chem.,* **115** (2015), 731–737.

[45] Xia T., Chen T., Wu W. and Zhou C., A deep learning-based framework for valence bond structure selection and weight prediction. *J. Chem. Theory Comput.,* **21** (2025), 1024.